



**A Search for  $ZH(\rightarrow l^+l^-b\bar{b})$  Production with the DØ Detector in  $p\bar{p}$  collisions at  $\sqrt{s} = 1.96$  TeV**

The DØ Collaboration  
URL <http://www-d0.fnal.gov>  
(Dated: July 26, 2006)

We report on a search for a Higgs boson produced in association with a  $Z$  boson at DØ in  $p\bar{p}$  collisions at  $\sqrt{s} = 1.96$  TeV at the Fermilab Tevatron collider. Events containing  $Z \rightarrow e^+e^-$  or  $\mu^+\mu^-$ , and two  $b$ -tagged jets are considered. Based on the integrated luminosity of 389 pb<sup>-1</sup> (320 pb<sup>-1</sup>) in the dielectron (dimuon) channel, good agreement between data and the expected background has been observed. The combined result for both dielectron and dimuon final states provides an upper limit on the  $ZH$  production cross section ranging from 4.5 pb to 6.1 pb for Higgs masses between 105 and 145 GeV.

*Preliminary Results for Summer 2006 Conferences*

## I. INTRODUCTION

One of the most sensitive production channels at the Tevatron for a Standard Model Higgs boson with a mass below approximately 140 GeV is the associated production of a Higgs boson with a  $Z$  boson. The  $Z$  boson decays into quark and anti-quark pair 69.8% of the time, but this four jet (additional two jets from  $H \rightarrow b\bar{b}$ ) final state is overwhelmed by a large background of multijet production. A search for  $ZH$  production in the  $\nu\bar{\nu}b\bar{b}$  final state, which has the next largest branching fraction, has been reported [1]. In this note we present for the first time a search for the  $ZH$  production in  $l^+l^-b\bar{b}$  final states, where the  $l$  is either an electron (dielectron channel) or a muon (dimuon channel). The product of cross section and branching fraction ( $\sigma(p\bar{p} \rightarrow ZH) \times Br(H \rightarrow b\bar{b})$ ) is predicted to be 0.12-0.012 pb for a Standard Model Higgs boson with a mass between 105 and 145 GeV.

The  $Z$  boson is reconstructed and identified from a pair of high  $p_T$  isolated dilepton with an invariant mass constraint. Events are required to have at least two  $b$ -tagged jets. We search for a  $H \rightarrow b\bar{b}$  resonance in the  $b$ -tagged dijet mass distribution. The dominant backgrounds result from the associated production of a  $Z$  boson with jets, among which the  $Zb\bar{b}$  production is an irreducible background. The other main backgrounds are  $t\bar{t}$ ,  $ZZ$ ,  $WZ$ , and multijet production from QCD processes. In order to isolate these background sources, an efficient  $b$ -tagging algorithm and a good dijet mass resolution are essential. The  $b$ -tagging efficiency and its fake rate are crucial elements of this analysis.

## II. DATA SAMPLE AND EVENT SELECTION

The DØ detector has a central-tracking system, consisting of a silicon microstrip tracker (SMT) and a central fiber tracker (CFT), both located within a 2 T superconducting solenoidal magnet [2], with designs optimized for tracking and vertexing at pseudorapidities  $|\eta| < 3$  and  $|\eta| < 2.5$ , respectively. A liquid-argon and uranium calorimeter has a central section (CC) covering pseudorapidities  $|\eta|$  up to  $\approx 1.1$ , and two end calorimeters (EC) that extend coverage to  $|\eta| \approx 4.2$ , with all three housed in separate cryostats [3]. An outer muon system, at  $|\eta| < 2$ , consists of a layer of tracking detectors and scintillation trigger counters in front of 1.8 T toroids, followed by two similar layers after the toroids [4]. Luminosity is measured using plastic scintillator arrays placed in front of the EC cryostats. The trigger and data acquisition systems are designed to accommodate the high luminosities of Run II.

The analyses are based on 389 pb<sup>-1</sup> and 320 pb<sup>-1</sup> of integrated luminosities for the dielectron and the dimuon channels, respectively, after the requirement of good data quality. The uncertainty of the luminosity measurement is 6.5% [5]. The dielectron sample is collected by the OR of unprescaled single electron triggers, while the dimuon sample uses one single muon trigger [6, 7].

In the subsections below, we describe event selection specific to each channel. The selection of hadronic jets is common to both analyses. A jet is reconstructed using the Run II cone algorithm with  $\Delta R = 0.5$  [8]. The jet must have  $p_T > 20$  GeV after the jet energy scale correction and a pseudorapidity of  $|\eta| < 2.5$ .

### A. Dielectron Sample

The dielectron events are selected by requiring two isolated electromagnetic (EM) clusters in the calorimeter. Each EM cluster must have  $p_T > 20$  GeV, and  $|\eta_{detector}| < 1.1$  or  $1.5 < |\eta_{detector}| < 2.5$ , where  $\eta_{detector}$  is the pseudorapidity measured at the calorimeter with respect to the coordinate origin, with at least one satisfying  $|\eta_{detector}| < 1.1$ . In addition, the shower shape developed in the calorimeter must be consistent with the expected behavior of an electron. At least one of the two EM clusters is also required to have an associated track with a momentum close to the EM cluster energy measured in the calorimeter. Figure 1 shows the invariant mass distribution reconstructed from the two electron candidates. Events with  $75 < M_{ee} < 105$  GeV are selected as  $Z$  candidates.

After selecting the  $Z$  candidates, we require the presence of at least two jets. The jets and electrons must be separated by  $\Delta R > 0.5$ .

### B. Dimuon Sample

In the dimuon sample selection, two isolated muons are required to be of opposite charge, have  $p_T > 15$  GeV, and  $|\eta| < 2.0$ . The muon trajectories in the muon detector must be matched to tracks found in the central tracking system (i.e. SMT+CFT), where the central track must have at least one hit in the SMT. In addition, the central tracks are required to have a distance of closest approach smaller than 0.25 cm with respect to the interaction vertex. The isolation is based on the measured energy in the calorimeter around the muon candidate, and the sum of  $p_T$  of tracks

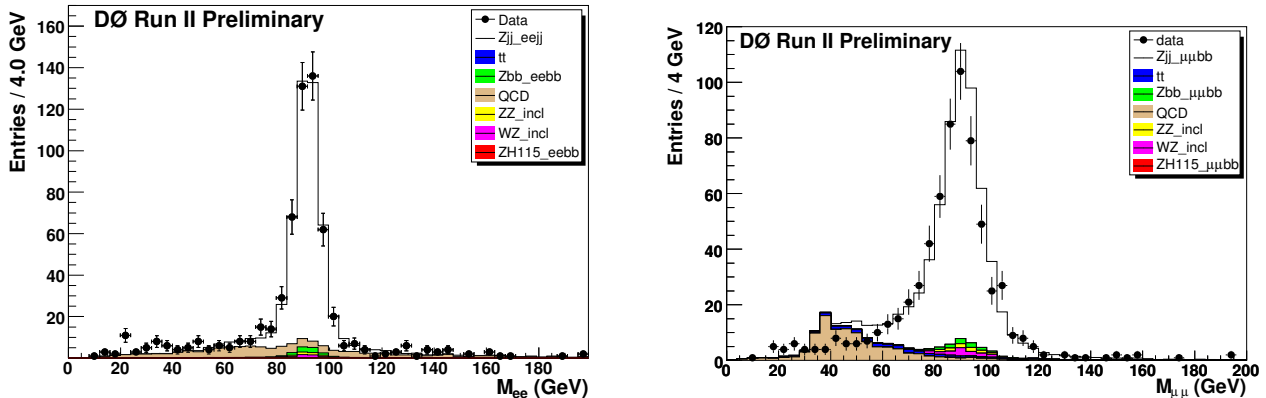


FIG. 1: The invariant mass distributions reconstructed from dielectron (left) and dimuon (right).

within the cone of  $\Delta R < 0.5$  with respect to the muon candidate. In order to select  $Z$  candidates, the opening angle of the dimuon in the transverse plane is required to be  $\Delta\phi > 0.4$ . Figure 1 shows the dimuon invariant mass. For the selection of  $Z$  candidates, the invariant mass of the dimuon system must be in range between 65 and 115 GeV. After selecting  $Z$  candidates, events are required to have at least two jets.

### III. SIMULATED EVENT SAMPLE

Using the CTEQ5L [9] leading-order parton distribution function, the following physics processes are simulated to estimate the signal acceptance and the number of background events:  $Z(\rightarrow l^+l^-)H(\rightarrow b\bar{b})$  by PYTHIA [10],  $Z(\rightarrow l^+l^-)bb$  by ALPGEN [11],  $Z(\rightarrow l^+l^-)jj$  including  $Z(\rightarrow l^+l^-)cc$  by ALPGEN,  $t\bar{t} \rightarrow l^+\nu b l^-\bar{\nu}b$  by ALPGEN,  $t\bar{t} \rightarrow bbjjl\nu$  by ALPGEN, inclusive  $ZZ$  by PYTHIA, and inclusive  $WZ$  by PYTHIA. The samples generated by ALPGEN are interfaced with PYTHIA for parton showering and hadronization. All these events are processed through the DØ detector simulation based on GEANT, the simulation of detector readout, and the reconstruction software. Finally the simulated events are weighted by the measured trigger efficiency and the ratio of selection efficiencies between data and simulation.

The absolute normalization of the background is according to NLO cross sections calculated by MCFM [12] with CTEQ6M, and the measured luminosity, except for  $Z(\rightarrow e^+e^-)jj$ . The normalization factor for the  $Z(\rightarrow e^+e^-)jj$  process is determined so that the number of events in data before  $b$ -tagging is consistent with the sum of the background events obtained by the absolute normalization and  $Z(\rightarrow e^+e^-)jj$  events. The systematic uncertainty on the NLO cross sections due to the scale dependence is estimated by varying the renormalization and factorization scales. The uncertainty due to the PDF is estimated by taking the maximum variation when the different eigenvectors for the parameterization are used. These two uncertainties are added in quadrature, leading to a total uncertainty of 6-19%, depending on the background process.

## IV. ANALYSIS

### A. Multijet (QCD) Background

There are 463  $Z + \geq 2$  jets events in the dielectron sample. The size of the multijet (QCD) contribution is estimated by fitting the dielectron mass distribution by a Breit-Wigner function convoluted with a Gaussian for the  $Z$  peak ( $N_Z$ ), and an exponential shape for QCD and Drell-Yan process ( $N_{QCD} + N_{DY}$ ). The fraction of Drell-Yan events is determined from the simulation. Out of 463 events, 28.0 events are estimated to be from multijet background.

The shape of the QCD background is obtained from data where the QCD contribution is enhanced by inverting the shower shape requirements for electron identification, and by removing the track match requirements. This sample does not have a  $Z$  peak in the dielectron mass distribution, and is used to predict the QCD background contribution

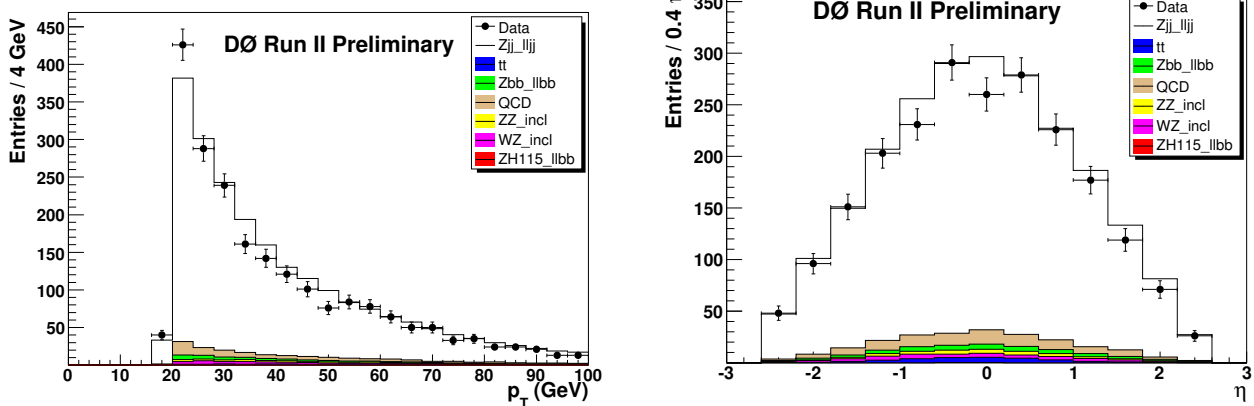


FIG. 2: Jet  $p_T$  (left) and  $\eta$  (right) distributions in  $Z(\rightarrow l^+l^-) + \geq 2$  jets events. The dots with error bars show data, and the open histogram shows the sum of expected contributions from signal and all backgrounds.

in the kinematical distributions.

There are 545  $Z + \geq 2$  jets events in the dimuon sample. The size of the QCD background contribution is estimated using two data samples; one with the muon isolation requirement, and the other without such a requirement. Assuming an identical muon isolation efficiencies for events from  $Z$  and Drell-Yan production, the unknowns before the  $b$ -tagging requirement are the number of QCD events ( $N'_{QCD}$ ) and the sum of number of  $Z$  and Drell-Yan events ( $N'_{Z+DY}$ ), if the isolation efficiencies can be measured from the other sample. The isolation efficiency for  $Z$  events is measured by taking the ratio of the  $Z$  yield in data with and without the isolation cut. The  $Z$  yield is obtained by fitting the dimuon mass distribution with a Gaussian for the  $Z$  peak and an exponential for the QCD and Drell-Yan events. The isolation efficiency for QCD events is estimated using QCD enhanced data, i.e. the data are collected by jet trigger, and selected by requiring at least one muon plus two or more jets. Since there are two equations for two unknowns, the system can be solved. Out of 545 events, 16.1 events are expected to result from QCD background.

Once we measure the isolation efficiency for the  $Z$  and Drell-Yan processes, we solve the similar equations after the  $b$ -tagging requirement. The unknowns this time are the isolation efficiency for QCD events, and the number of QCD events, because the isolation efficiency for  $Z$  or Drell-Yan processes, and the  $Z$  to Drell-Yan ratio do not depend on the  $b$ -tagging requirement, while the isolation efficiency for the QCD background depends on the  $b$ -tagging requirement.

Figure 2 shows the  $p_T$  and  $\eta$  distributions for jets in the  $Z + \geq 2$  jets events, where the dielectron and dimuon samples are combined. Figure 3 shows  $\Delta R$  between the two jets, and the dijet invariant mass distributions. The reasonable agreements between the data and the expectation are observed in these distributions.

## B. $b$ -jet Tagging

The hadronic jet is defined as “taggable” if it is associated with a cluster of tracks ( $\equiv$  track jet) within  $\Delta R < 0.5$ . The track jet is found by applying a cone track clustering algorithm with the size  $\Delta R = 0.5$ . The track jet is required to have at least two tracks, where the seed track must have  $p_T > 1$  GeV, and the other  $p_T > 0.5$  GeV. Each track must be within 2 cm of the interaction vertex in  $z$  and have at least one SMT hit.

The  $b$ -jet tagging algorithm used in both the dielectron and the dimuon samples is based on the probability to observe the lifetime of  $b$ -hadrons estimated from the tracks associated with a given taggable jet [13]. A small probability ( $p$ ) corresponds to jets having tracks with large impact parameters resulting from  $b$ -hadron decays. We have studied different requirements on the jet lifetime probability between  $p < 0.001$  (tightest) and  $p < 0.04$  (loosest).

The statistical significance, defined as the number of expected  $ZH$  events divided by the square root of the number of total background events, is investigated by comparing six different requirements on the jet lifetime probability and the number of  $b$ -tagged jets, leading to 12 combinations. The optimal selection has been identified as double  $b$ -tagging with a requirement on the lifetime probability smaller than 0.04. With this requirement, the  $b$ -jet tagging efficiency

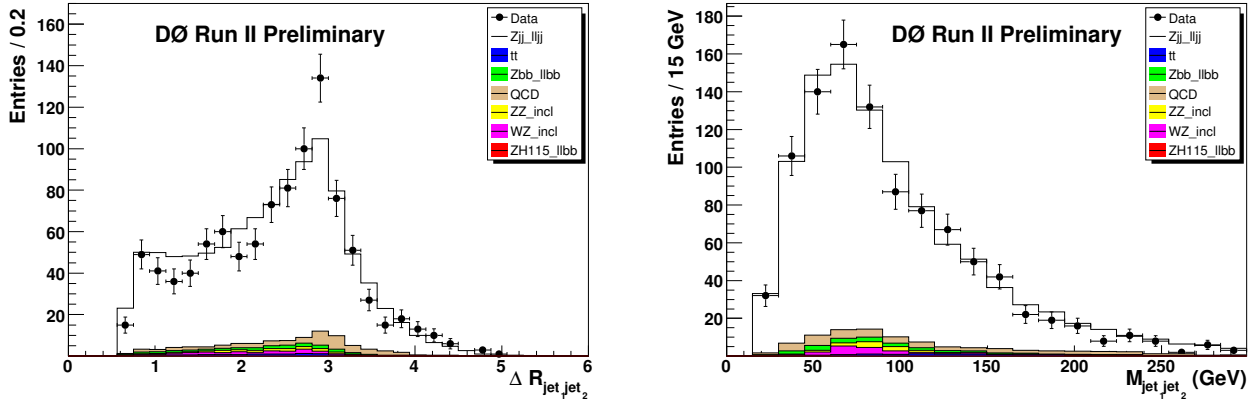


FIG. 3:  $\Delta R$  between two jets (left) and dijet mass invariant mass (right) in distributions in  $Z(\rightarrow l^+l^-) + \geq 2$  jets events. The dots with error bars show data, and the open histogram shows the sum of expected contributions from signal and all backgrounds.

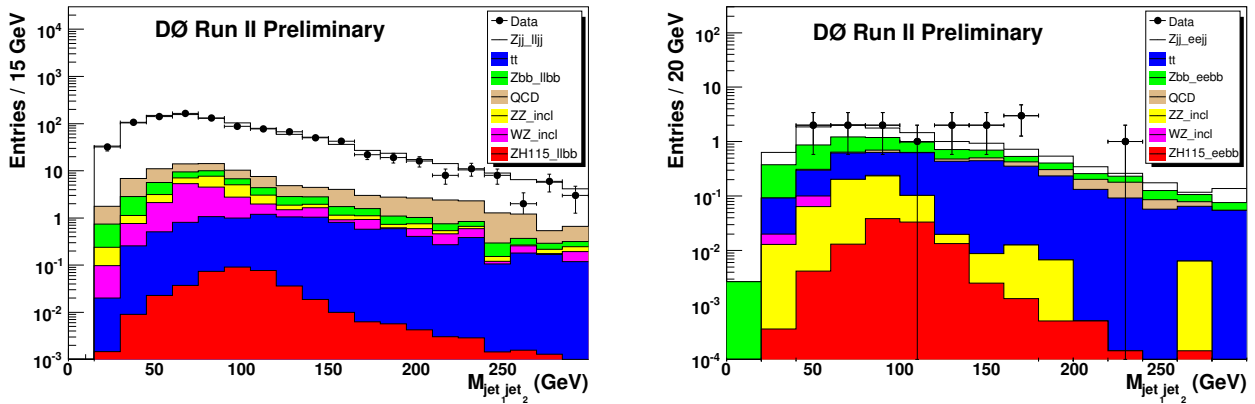


FIG. 4: Dijet invariant mass distributions reconstructed from the two leading  $p_T$  jets before the  $b$ -tagging requirement (left), and the same distribution reconstructed from  $b$ -tagged jets (right). The dielectron and dimuon samples are combined.

per taggable jet is measured to be 69%, while the light jet tagging rate per taggable jet is 4%, for any taggable jets with  $35 < p_T < 55$  GeV and  $|\eta| < 1.2$  [13].

After the application of the selection criteria, the acceptance for a Higgs signal ( $M_H = 115$  GeV) including all of the efficiency corrections multiplied by the branching fraction of  $Z \rightarrow l^+l^-$  is 0.15% for the dielectron sample, and 0.17% for the dimuon sample. Figure 4 shows the dijet invariant mass distribution reconstructed from two leading  $p_T$  jets before  $b$ -tagging, and from two  $b$ -tagged jets where two leading  $p_T$  jets are used when two or more jets are  $b$ -tagged. In Table I, the number of observed events along with the expected number of background events are summarized.

TABLE I: Number of observed and expected background events.

	$Z + \geq 2$ jets			with 2 $b$ -tags		
	$Z \rightarrow e^+e^-$	$Z \rightarrow \mu^+\mu^-$	$Z \rightarrow l^+l^-$	$Z \rightarrow e^+e^-$	$Z \rightarrow \mu^+\mu^-$	$Z \rightarrow l^+l^-$
$Zbb$	7.9	8.9	16.8	1.7	1.4	3.1
$Zjj$	416	521	937	1.5	3.0	4.5
$t\bar{t}$	2.4	9.0	11.4	0.8	2.9	3.7
$ZZ + WZ$	8.1	18.3	26.4	0.22	0.37	0.59
QCD	28.0	16.1	44.1	0.18	0.41	0.59
Expected total background	463	573	1048	4.5	8.1	12.6
Observed events	463	545	1008	5	10	15

### C. Systematic Uncertainties

The following are the sources of the systematic uncertainties.

- Trigger efficiency: Because the single lepton triggers are used for the process involving two leptons, the trigger efficiency is very high, especially for the leptons from  $Z$  decays due to its high  $p_T$ . The resulting uncertainty is about 1%.
- Lepton reconstruction and identification efficiencies: This includes the uncertainty of the central track matching efficiency that is used in both electron and muon identification. The uncertainty in the dielectron sample is 4-5% for signal depending on the Higgs mass, and 4-6% for background depending on the process. The uncertainty in the dimuon sample is 11-12% for signal depending on mass, and 11-16% for background depending on the process.
- Lepton energy and resolution: 2%.
- Jet reconstruction and identification efficiencies: 8% for signal, and 5-11% for background.
- Jet energy scale: 7% for signal, and 10% for background.
- Taggability: 4%.
- $b$ -tagging rate: 8% for signal, and 9-11% for background.
- Cross sections for the simulated events: 7% for signal, and 6-19% for background.
- QCD background estimation: 50% in the dielectron sample, and 275% in the dimuon sample. Although the relative uncertainty is large, the absolute uncertainty is small because of the small contributions.

For a  $ZH$  signal or a given background process, the total uncertainty is obtained by adding each contribution above in quadrature. The total systematic uncertainty for  $ZH$  production is 19%. In order to get the total uncertainty for the background processes, the correlations among the individual uncertainties must be properly taken into account. This is performed when getting the combined cross section limit.

There is an additional 6.5% uncertainty from the luminosity measurement.

### V. CROSS SECTION LIMIT

We search for an excess of events in the dijet invariant mass distribution. The search window is defined to be  $\pm 1.5\sigma$ , where the  $\sigma$  is the dijet mass resolution obtained in the simulated events around the expected peak by Higgs for a given hypothetical mass. The search windows are summarized in Table II. The mass peak in the dijet mass spectrum

TABLE II: The dijet mass window to search for Higgs signal.

Higgs mass (GeV)	dielectron sample (GeV)	dimuon sample (GeV)
105	65-113	65-118
115	72-125	70-128
125	75-136	78-137
135	82-143	84-147
145	87-156	92-160

is expected to be smaller than the hypothetical Higgs mass because the jet energy is corrected to the particle level, e.g. energy leakage outside the cone due to final state radiation is not corrected. The observed number of events and the expected background contributions are summarized in Table III, IV, and V. No significant excess is observed in any mass window, and hence the upper limits on  $\sigma(pp \rightarrow ZH) \times Br(H \rightarrow b\bar{b})$  are set at the 95% confidence level, as also shown in Table III, IV, and V. Based on  $CL_s$  method, the dijet invariant mass distributions are used to calculate all the limits in these Tables, i.e. both in the individual analyses and in the combined result [14].

Figure 5 shows the observed and expected cross section limits obtained from the combination of the dielectron and the dimuon channels as a function of the Higgs mass. The Standard Model prediction is also shown.

TABLE III: The results of  $Z(\rightarrow e^+e^-)H$  search for various hypothetical Higgs masses. The number of observed and expected events are listed, as well as the observed and expected upper limits on  $\sigma(p\bar{p} \rightarrow ZH) \times Br(H \rightarrow b\bar{b})$ .

Higgs mass (GeV)	105	115	125	135	145
Expected $ZH$	0.07	0.05	0.04	0.02	0.01
$Zb\bar{b}$	0.6	0.6	0.6	0.6	0.6
$Zjj$	0.4	0.2	0.3	0.4	0.4
$t\bar{t}$	0.3	0.3	0.3	0.3	0.3
$ZZ + WZ$	0.1	0.1	0.1	0.1	0.1
QCD	0.04	0.03	0.09	0.04	0.09
Expected total background	1.4	1.3	1.4	1.4	1.5
Observed events	2	2	2	2	1
Observed cross section limit (pb)	7.8	7.9	5.5	4.5	4.1
Expected cross section limit (pb)	6.0	6.5	5.3	4.4	4.0

TABLE IV: The results of  $Z(\rightarrow \mu^+\mu^-)H$  search for various hypothetical Higgs masses. The number of observed and expected events are listed, as well as the observed and expected upper limits on  $\sigma(p\bar{p} \rightarrow ZH) \times Br(H \rightarrow b\bar{b})$ .

Higgs mass (GeV)	105	115	125	135	145
Expected $ZH$	0.06	0.05	0.03	0.02	0.01
$Zb\bar{b}$	0.6	0.6	0.5	0.5	0.4
$Zjj$	1.2	1.1	0.9	1.0	0.9
$t\bar{t}$	1.0	1.1	1.1	1.2	1.2
$ZZ + WZ$	0.3	0.2	0.2	0.2	0.1
QCD	0.04	0.04	0.03	0.03	0.04
Expected total background	3.1	3.1	2.8	2.8	2.7
Observed events	3	3	4	5	6
Observed cross section limit (pb)	11.9	11.2	11.7	10.7	11.1
Expected cross section limit (pb)	10.3	12.6	11.4	6.2	5.7

## VI. SUMMARY

Using 320-389  $\text{pb}^{-1}$  of data, a search for  $ZH$  production followed by the decays of  $Z \rightarrow l^+l^-$  and  $H \rightarrow b\bar{b}$  has been conducted. In events with  $Z$  boson +  $\geq 2$  jets, a search for an excess over the expected background level has been performed in the dijet invariant mass spectrum of the two leading  $b$ -tagged jets. Both the number of events and the kinematical distributions are consistent with the expectation of the background hypothesis. In absence of a signal, 95% confidence level upper limits on  $\sigma(p\bar{p} \rightarrow ZH) \times Br(H \rightarrow b\bar{b})$  are set to 4.5-6.1 pb for Higgs boson with masses between 105 GeV and 145 GeV.

TABLE V: The results of  $Z(\rightarrow l^+l^-)H$  search for various hypothetical Higgs masses. The number of observed and expected events are listed.

Higgs mass (GeV)	105	115	125	135	145
Expected $ZH$	0.13	0.09	0.07	0.04	0.02
$Zb\bar{b}$	1.2	1.2	1.1	1.0	1.0
$Zjj$	1.6	1.3	1.2	1.4	1.3
$t\bar{t}$	1.3	1.4	1.4	1.5	1.5
$ZZ + WZ$	0.4	0.3	0.3	0.3	0.2
QCD	0.09	0.07	0.12	0.07	0.13
Expected total background	4.6	4.3	4.1	4.3	4.1
Observed events	5	5	6	7	7
Observed cross section limit (pb)	6.1	6.1	5.0	4.5	4.7
Expected cross section limit (pb)	4.7	4.7	4.0	3.2	2.9

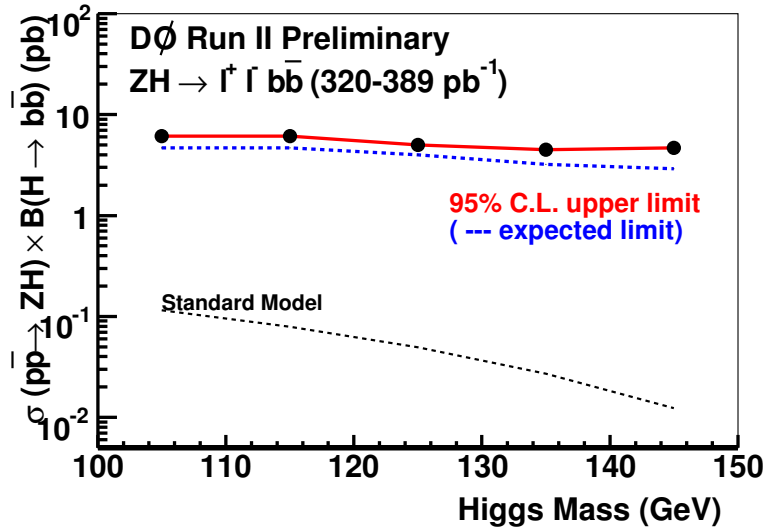


FIG. 5: The 95% confidence level upper limits on  $\sigma(p\bar{p} \rightarrow ZH) \times Br(H \rightarrow b\bar{b})$  for different Higgs mass. The limits are derived from the combination of the  $Z \rightarrow e^+e^-$  and the  $Z \rightarrow \mu^+\mu^-$  samples.

#### Acknowledgments

We thank the staffs at Fermilab and collaborating institutions, and acknowledge support from the DOE and NSF (USA); CEA and CNRS/IN2P3 (France); FASI, Rosatom and RFBR (Russia); CAPES, CNPq, FAPERJ, FAPESP and FUNDUNESP (Brazil); DAE and DST (India); Colciencias (Colombia); CONACyT (Mexico); KRF and KOSEF (Korea); CONICET and UBACyT (Argentina); FOM (The Netherlands); PPARC (United Kingdom); MSMT (Czech Republic); CRC Program, CFI, NSERC and WestGrid Project (Canada); BMBF and DFG (Germany); SFI (Ireland); Research Corporation, Alexander von Humboldt Foundation, and the Marie Curie Program.

- 
- [1] M. Tomoto, DØ note 4774 (2005).
  - [2] DØ Collaboration, V. Abazov *et al.*, “The Upgraded DØ Detector”, accepted by Nucl. Instrum. Methods Phys. Res. A.
  - [3] DØ Collaboration, S. Abachi *et al.*, Nucl. Instrum. Methods Phys. Res. A **338**, 185 (1994).
  - [4] V. Abazov *et al.*, “The Muon System of the Run II DØ Detector”, physics/0503151.
  - [5] Luminosity ID group: [http://www-d0.fnal.gov/phys\\_id/luminosity/data\\_access/](http://www-d0.fnal.gov/phys_id/luminosity/data_access/)
  - [6] J. Heinmiller, A. Stone, and N. Varelas, DØ note 5185 (2006).
  - [7] H. Dong and J.D. Hobbs, DØ note 5107 (2006).
  - [8] G.C. Blazey *et al.*, Run II Jet Physics, hep-ex/0005012.
  - [9] H.L. Lai *et al.*, Phys. Rev. D**55**, 1280 (1997).
  - [10] T. Sjöstrand *et al.*, Comput. Phys. Commun. **135**, 238 (2001).
  - [11] M.L. Mangano, M. Moretti, F. Piccinini, R. Pittau, and A. Polosa, J. High Energy Phys. 07 (2003) 001.
  - [12] J. Campbell and K. Ellis, MCFM, *Monte Carlo for FeMtobarn processes*, <http://mcfm.fnal.gov/>
  - [13] D. Bloch *et al.*, DØ note 4348 (2004). D. Bloch and B. Clément, DØ note 4824 (2005).
  - [14] W. Fisher, DØ note 4975. The DØ collaboration, DØ note 5056.